A Comparative Analysis of Nitride based Compound Semiconductor Resonant Tunnelling Diode

A Report for End Semester Evaluation submitted to
Indian Institute of Technology, Kharagpur
in partial fulfilment for the award of the degree of
Bachelor of Technology (Hons.)
in

Electronics and Electrical Communication Engineering

by
DEBANJAN NANDI (10EC35026)

Under the supervision of
Prof. Dhrubes Biswas

Department of Electronics and Electrical Communication Engineering,

Indian Institute of Technology Kharagpur,

Spring Semester 2013-14

Declaration

I certify that

a) The work contained in this report has been done by me under the guidance of my supervisor.

b) The work has not been submitted to any other Institute for any degree or diploma.

c) I have conformed to the norms and guidelines given in the Ethical Code of Conduct of the Institute.

d) Whenever I have used materials (data, theoretical analysis, figures and text) from other sources, I have given due credit to them by citing them in the text of the thesis and giving their details in the references. Further, I have taken permission from the copyright owners of the sources, whenever necessary.

Date:
Place:

Debanjan Nandi
10EC35026

DEPARTMENT OF ELECTRONICS AND ELECTRICAL COMMUNICATION ENGINEERING

INDIAN INSTITUTE OF TECHNOLOGY, KHARAGPUR

Certificate

This is to certify that the project report entitled "*A Comparative Analysis of Nitride based Compound Semiconductor Resonant Tunnelling Diode*" submitted by Debanjan Nandi (Roll No. 10EC35026) to Indian Institute of Technology, Kharagpur towards partial fulfilment of requirements for the award of the degree of Bachelor of Technology (Hons.) in the Department of Electronics and Electrical Communication Engineering, is a record of bona fide work carried by him under my supervision and guidance during academic session 2013 – 14.

Date: Prof. Dhrubes Biswas

Place:

Acknowledgement

The success and the final outcome of this project required a lot of guidance and assistance from many people and I am extremely fortunate to have got this all along the completion of this project work. Whatever I have done has been possible only due to such support and I would never forget to thank them.

Firstly, I respect and thank my project guide **Prof. Dhrubes Biswas,** Department of Electronics and Electrical Communication Engineering, Indian Institute of Technology, Kharagpur for permitting me to work on this challenging project of his, under his esteemed guidance.

I wish to express my deepest gratitude to **Prof. Tarun Kanti Bhattacharya,** Department of Electronics and Electrical Communication Engineering, Indian Institute of Technology, Kharagpur for extending me the facilities in the Advanced VLSI Design Laboratory.

I also owe my profound gratitude to **Ms. Subhra Chowdhury, Research Scholar** at the Advanced Technology Development Centre, Indian Institute of Technology, Kharagpur who took a keen interest in my project work and guided me all along by providing me with all the information necessary for carrying out my research. Her constant motivation and words of encouragement was what kept me going through difficult times.

Lastly, I would like to convey my heartfelt thanks to all the other Research Scholars, Technicians and Staff at the Advanced Technology Development Centre for providing me with a helping hand in times of need.

Contents

Abstract

Resonant Tunnelling diodes are commonly formed from heterostructures consisting of layers of GaAs/AlAs, InAs/AlSb, or InAs/GaSb on GaAs or InP substrates, depending upon criteria such as lattice matching. However, III- nitrides such as AlGaN / GaN have gained a lot of interest recently for resonant tunnelling diodes (RTDs). This is primarily because of their wide bandgap, large conduction band offset, and high carrier mobility. It thus helps in creation of larger PVRs and quantum behaviour at much higher temperature than any other III-V systems. Thus such devices can offer higher power, higher frequency room- temperature operations than other members of the III-V family.

However, the lattice mismatch and strain between AlGaN and GaN layers in AlGaN / GaN RTDs gives rise to the much undesired piezoelectric polarization charges across the interfaces which eventually degrades the performance of RTD by providing asymmetric current voltage characteristics. Therefore, in order to get a reliable, reproducible Negative differential region as well as symmetric current-voltage characteristics, it is absolutely necessary to use a material which would minimise lattice mismatch and hence reduce strain, thereby reducing piezoelectric polarization charges. $Al_{0.83}In_{0.17}N$ alloy which has a lattice constant = 3.187 Å [19], is thereby used since it is lattice-matched with GaN (lattice constant = 3.190 Å [19]). InAlN / GaN also has spontaneous polarization larger than total of spontaneous and piezoelectric polarization in typical AlGaN / GaN heterostructure, which results in a higher 2DEG charge density at the interface. The large polarization discontinuity between InAlN / GaN enables higher charge densities as well as larger band offset to GaN well than in the conventional AlGaN /GaN structures, significantly reducing the access resistance in these devices, and the lack of strain in AlInN reduces device degradation processes and leads to better structure and reliability. Therefore, it is an effective approach to improve the performance of RTD by employing a nearly lattice-matched InAlN / GaN structure to lower dislocation density and weaken piezoelectric field at the heterointerface [19].

In this project, I have attempted to analyse the current – voltage characteristics of AlGaN / GaN resonant tunnelling diodes through Matlab and ATLAS simulation. A current – voltage simulation of AlInN / GaN resonant tunnelling diode is done next, followed by a comparison of $Al_{0.2}Ga_{0.8}N$ / GaN and $Al_{0.83}In_{0.17}N$ / GaN RTDs. Polarization charges, which play a crucial role in all III-V nitride based heterostructures, have been taken into consideration for calculations.

Chapter 1: Resonant Tunnelling Diodes

1.1. Tunnelling Basics:

Tunnelling is a purely quantum phenomena which enable electrons to penetrate potential barriers even though it is classically forbidden. The scheme is illustrated in Figure 1.1. Classically, the electron would be reflected if $E<V_0$ but due to tunnelling, there is a probability that the electron penetrates the barrier. On the other hand, classically, if the electron has energy $E>V_0$, it is certain to be transmitted through the barrier, but in quantum mechanics there is a probability of reflection even when the energy exceeds the barrier height.

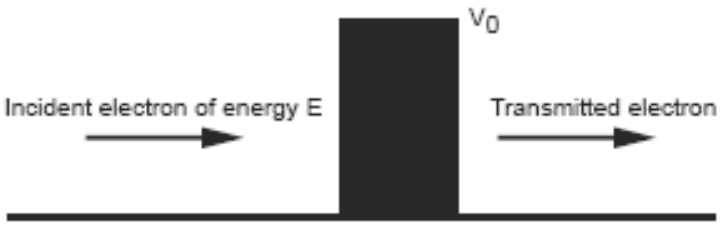

Figure 1.1 The basics of Tunnelling. An electron of energy E is incident on a barrier of potential V_0. Classically, the electron is reflected when $E<V_0$, quantum mechanically, there is a probability that the electron is transmitted through the barrier.

Tunnelling though a potential barrier is characterised by a transmission coefficient T so that $0 \leq T \leq 1$. The transmitted wavefunction ψ_T is thus given by $T\psi_I$, where ψ_I is the wavefunction of the incident particle.

Figure 1.2 Tunnelling through double barrier. When $E<< V_0$, the region between both the barriers will act as a quantum well with quantized energy levels which facilitate resonance tunnelling

A double barrier structure, like the one shown in Figure 1.2, gives rise to the QM phenomena called resonant tunnelling. If the transmission coefficients of the left and right barriers, T_L and T_R respectively, are both much smaller than unity, a quantum well arises in between the barriers. This means that the energy levels in the well will be quantized. Strictly speaking this is not entirely true because T_R and T_L are in fact, of course, not equal to zero. This means that the energy levels and the bound states in the well will be referred to as quasi-bound states. When an electron with an energy which is not coincident with one of the quasi-quantized levels in the well is incident on the barrier/well complex the global transmission coefficient T_G is much smaller than unity. If however, the electron energy coincides with one of the energy levels in the well, resonance occurs and the electron can be transmitted with a

transmission coefficient on the order of unity. This is the type of structure which is utilized in resonant tunnelling diodes.

1.2. Resonant Tunnelling Diodes

Typically, in resonant tunnelling diodes, the electrons come from a doped semiconductor or a metal material. Resonant Tunnelling diodes consists of two heavily doped, narrow energy-gap materials encompassing an emitter region, a quantum well in between two barriers of large band gap material, and a collector region, as shown in the Figure 1.3. The energy of the electrons are raised by applying a voltage across the structure.

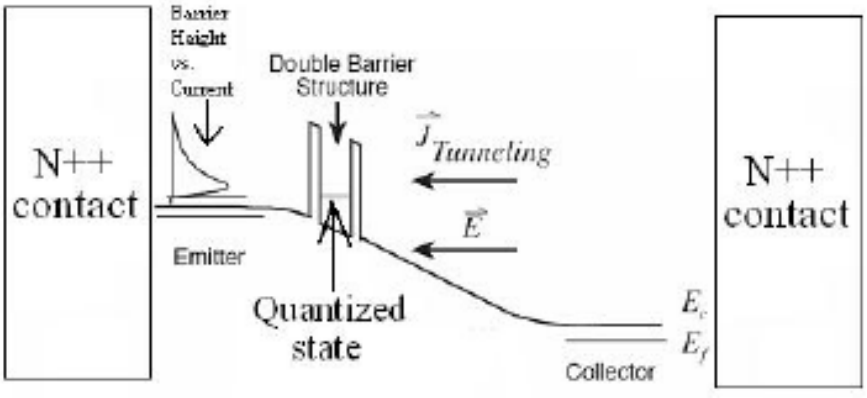

Figure 1.3 Structural Diagram of RTD [5]

When there is no forward bias, most of the electrons and holes are stationary forming an accumulation layer in the emitter and collector region respectively. As a forward voltage bias is applied, an electric field is created that cause the electrons to move from the emitter to the collector by tunnelling through the scattering states within the quantum well. These quasi bound energy states are the energy states that allow for electrons to tunnel through creating a current. As more and more electrons are able to tunnel through the well, resulting in an increase in the current as the applied voltage is increased. When the electric field increase to the point where the energy level of the quasi-bound state of the well, the current reaches a maximum, as shown in Fig 1.4.

Resonant tunnelling occurs at specific resonant energy levels corresponding to the doping levels and width of the quantum well. As the applied voltage continues to increase, more and more electrons are gaining too much energy to tunnel through the well, and the current is decreased. After a certain applied voltage, current begins to rise again because of substantial thermionic emission where the electrons can tunnel through the non-resonant energy levels of the well. This process is produces a minimum “valley” current that can be classified as the leakage current, as shown in Figure 1.4

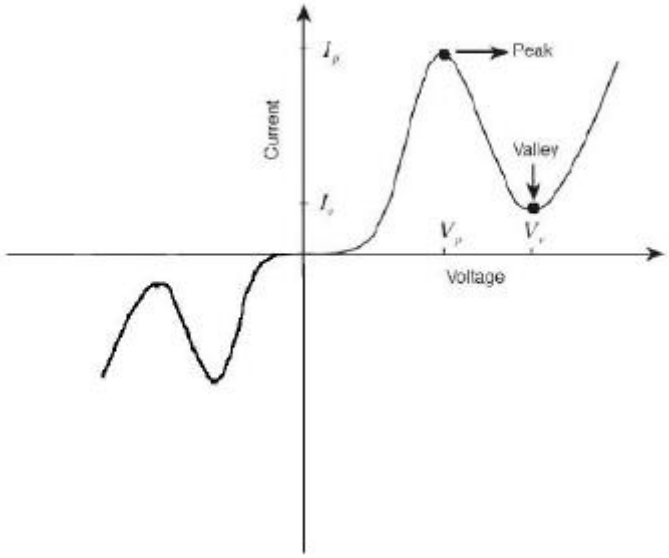

Figure 1.4 I-V characteristics of RTD

Figure 1.5 shows the effect of voltage across the RTD on the double barrier structure. As is apparent, the symmetry in the system is destroyed because the two barriers no longer have the same height and therefore not the same transmission coefficient. This obviously has an impact on the energy levels in the well, and in general it will be much more difficult to obtain a global transmission coefficient $T_G \approx 1$.

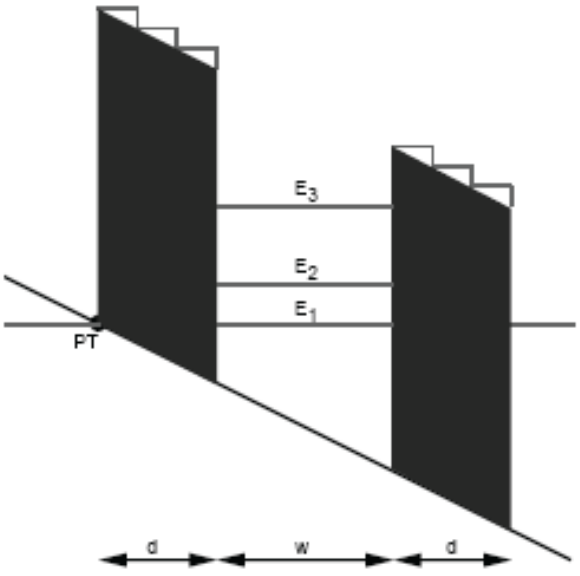

Figure 1.5 Double Barrier with Applied Potential

Chapter 2: Transfer Matrix Formulation

2.1. Constant Potential

In this section the transfer matrix formulation of the quantum tunnelling will be described and the results shown. To describe the technique the simple scenario in Figure 2.1 will be considered.

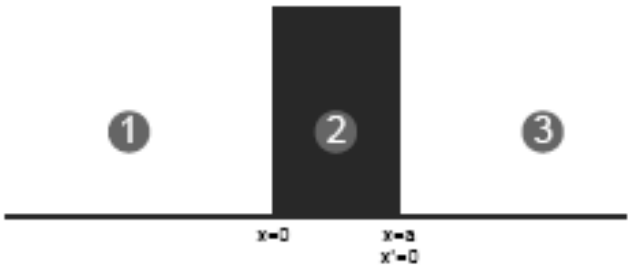

Figure 2.1 Tunnelling through a single barrier

In region 1, the wave function is termed as ψ_1 and the potential is zero, in region 2, the wave function is termed ψ_2 and the potential is V_0 and in region 3 the wave function is termed ψ_3 and the potential is again zero. The solutions to the Schrodinger equation in these regions are

$$\Psi_1 = Ae^{ik_1x} + Be^{-ik_1x} \quad (1)$$

$$\Psi_2 = Ce^{ik_2x} + De^{-ik_2x} \quad (2)$$

$$\Psi_3 = Ee^{ik_3x} + Fe^{-ik_3x} \quad (3)$$

where, $k_i=\sqrt{2m(E-V_i)}$

The wave function and its derivative is required to be continuous at the discontinuity between adjacent regions, i.e. $x=0$ and $x=a$. This requirement is imposed in order to avoid abrupt changes in probability density. Using these two continuity conditions between 1 and 3 yields the two equations.

$$A + B = C + D \quad (4)$$

$$ik_1A - ik_2B = ik_3C - ik_4D \quad (5)$$

These conditions can be written in the matrix form

$$\begin{pmatrix} 1 & 1 \\ ik_1 & -ik_1 \end{pmatrix} \cdot \begin{pmatrix} A \\ B \end{pmatrix} = \begin{pmatrix} 1 & 1 \\ ik_2 & -ik_2 \end{pmatrix} \cdot \begin{pmatrix} C \\ D \end{pmatrix}$$

Using the inverse matrix theorem an expression connecting (A, B) with (C, D) can be obtained

$$\begin{pmatrix} A \\ B \end{pmatrix} = \frac{1}{2(k_1)} \begin{pmatrix} k_1 + k_2 & k_1 - k_2 \\ k_1 - k_2 & k_1 + k_2 \end{pmatrix} \cdot \begin{pmatrix} C \\ D \end{pmatrix} = M_{12} \cdot \begin{pmatrix} C \\ D \end{pmatrix}$$

The matrix M_{12} is known as the discontinuity matrix and it connects the wave function in the region 1 with wave function in the region 2, i.e. it describes the propagation of the wave function across a boundary.

The wave function is also required to be continuous across the boundary between region 2 and region 3. A new coordinate system is chosen so that $x' = 0$ at $x = a$ and the primed coordinate system is therefore related to the unprimed one by $x' = x - a$. To obtain the connection between the primed and unprimed wave function, the relation $\psi_2(x) = \psi'_2(x - a)$ is exploited

$$Ce^{ik_2x} + De^{-ik_2x} = C'e^{ik_2(x-a)} + D'e^{-ik_2(x-a)} \qquad (6)$$

Or written in the matrix form as

$$\begin{pmatrix} C \\ D \end{pmatrix} = \begin{pmatrix} e^{ik_2a} & 0 \\ 0 & e^{-ik_2a} \end{pmatrix} \cdot \begin{pmatrix} C' \\ D' \end{pmatrix} = M_p \cdot \begin{pmatrix} C \\ D \end{pmatrix}$$

Where, M_p is called the propagation matrix. It describes the propagation of the wave function between two boundaries and ***a*** is the distance between the points to be connected. In the case considered here, it describes the propagation of the wave function inside the barrier. When inside a barrier the k_i's are purely imaginary and the matrix becomes an operator scaling the operand by an exponentially decaying factor, which is the behaviour expected from a matrix describing propagation within a potential barrier. The matrix M_p can equally well be used to describe propagation inside a quantum well, in which case it modulates the operand by a plane wave, i.e. a phase-shift operator.

As an example, consider a situation like the one depicted in Figure 1.2. The left region of zero potential is labelled 1, the left barrier 2, the zero potential well 3, the right barrier 4 and the right of the zero potential 5. The system matrix is then given by

$$M_s = M_{12} \cdot M_B \cdot M_{23} \cdot M_w \cdot M_{34} \cdot M_B \cdot M_{45} \qquad (7)$$

The coefficients of (A, B) are therefore related to the coefficients (F, G) by

$$\begin{pmatrix} A \\ B \end{pmatrix} = M_s \cdot \begin{pmatrix} F \\ G \end{pmatrix}$$

The transmission coefficient of a barrier is equal to the square of the transmitted wave, divided by the square of the incoming wave. Setting G equal to zero because there is no incoming wave in the region5 the transmission coefficient through the whole system can be expressed as

$$T = \frac{\left|Fe^{ik_1x}\right|^2}{\left|Ae^{ik_1x}\right|^2} = \frac{F^*F}{A^*A}$$

Where * denotes the complex conjugate. Therefore,

$$T = \frac{F^*F}{(M_{s,11}F)^*(M_{s,11}F)} = \frac{1}{M_{s,11}{}^*M_{s,11}} = \frac{1}{\left|M_{s,11}\right|^2}$$

2.2. Arbitrary Potential

In the last section the potential considered was of a rectangular shape. In this section the results will be generalised to potential of arbitrary shape. The generalisation is not very difficult, the arbitrary potential is divided into a number of square potential barrier divisions of width *d* and separated by quantum by quantum well of width *w*. the system matrix is then calculated in the limit when *w* goes to zero corresponding to the barriers being infinitely close together (no quantum well between them). The matrix of an arbitrary barrier can then be calculated by

$$\mathrm{M_s} = \mathrm{M_{12}}.\,\mathrm{M_B}.\,\mathrm{M_{23}}.\,\mathrm{M_w}.\,\mathrm{M_{34}}.\,\mathrm{M_B}.\,\mathrm{M_{45}}\ldots\ldots$$

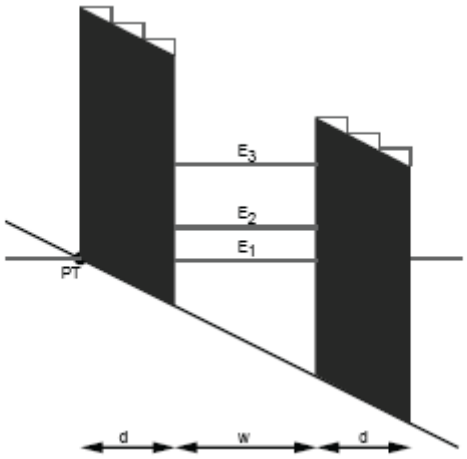

Where $\mathrm{M_s}$ denotes the system matrix i.e. the matrix describing the propagation of the wave function through the whole system of barriers and wells. When the well depth goes to zero, the propagation matrices $\mathrm{M_{wx}}$ become unit matrices, as "*a*"becomes equal to zero.

The product of two matrices $\mathrm{M_{23}}.\mathrm{M_{34}}$ is a product of two discontinuity matrices. Multiplying these two matrices gives the matrix

$$M_{24} = M_{23}M_{34} = \frac{1}{2(k_2)}\begin{pmatrix} \mathrm{k_2} + \mathrm{k_4} & \mathrm{k_2} - \mathrm{k_4} \\ \mathrm{k_2} - \mathrm{k_4} & \mathrm{k_2} + \mathrm{k_4} \end{pmatrix}$$

Taking the limit when d (the barrier division width) goes to zero would produce an infinite number of matrices, so a finite width is chosen. The number of square barriers to divide each arbitrary barrier into to obtain correct results depend on the arbitrariness of the barrier. A parabolic shaped potential requires more divisions than a barrier where one sides is at only a slightly lower potential than the other side to get valid results.

2.3. Current in Resonant Tunnelling Diode

To calculate the tunnelling current through the multi-barrier complex, it is necessary to consider the Fermi distributions in the semiconductor or metal structures surrounding the barriers. The Fermi distributions give the probability that an electron state of a certain energy is occupied. If the Fermi distribution on the left hand side is termed f_L and the distribution on the right hand side f_R the tunnelling current is proportional to

$$I \propto \int_0^\infty T(E)[f_L(E) - f_R(E)]\, D(E)dE$$

Where D (E) is the density of states (DOS) and T (E) is the probability of tunnelling for an electron of energy E. For an electron to travel through the barrier complex there has to be an electron with appropriate energy in the electron donor material and an unoccupied electron level for this electron in the acceptor material. This behaviour is taken care of by the term in the sharp parentheses. When $f_L(E) = 1$ and $f_R(E) = 0$ and electron can travel from left to right. When $f_L(E)$ and $f_R(E)$ are both zero or both unity the electron with energy E does not contribute to the total current. The Fermi distributions for the left and right hand sides are given by

$$f_L(\mathrm{E}) = (e^{(E+eV-E_f)/kT} + 1)^{-1} \quad \text{and} \quad f_R(\mathrm{E}) = (e^{(E-E_f)/kT} + 1)^{-1}$$

Where E_f is the Fermi energy under zero applied field. Electrons in the left hand side will have an energy which differs from the zero applied field case by – eV. Assuming that a potential V < 0 is applied to the left metal (the right metal being grounded), the electrons are raised to higher energy levels and the Fermi energy increases accordingly. This means that the Fermi energy will be higher in the left metal than in the right one, thus the difference between the Fermi distributions on the left and right. The density of states D (E) for a free electron Fermi gas in three dimensions is given by

$$D(E) = \frac{\sqrt{2}m_e^{3/2}}{\pi^2\hbar^3}\sqrt{E - E_c}\,\theta(E - E_c)$$

Where E_c is the energy of the conduction band bottom and $\theta(E - E_c)$ is the Heaviside step function. When the energy E is lower than the conduction band edge the density of states is zero. Considering all measurements with respect to the conduction band bottom, the equation for current becomes

$$I \propto \int_0^\infty T(E)[f_L(E) - f_R(E)]\sqrt{E}\, dE$$

Where the constants of the DOS expression has been omitted because they make no difference for the proportionality.

Chapter 3: AlGaN /GaN/ AlGaN Resonant Tunneling Diode

Resonant Tunneling diodes are commonly formed from heterostructures consisting of layers of GaAs/AlAs, InAs/AlSb, or InAs/GaSb on GaAs or InP substrates, depending upon criteria such as lattice matching. At room temperature, GaAs/AlAs typically have a peak-to-valley current ratio (PVR) of around 3. However, III- nitrides have gained a lot of interest recently for resonant tunnelling diodes (RTDs). This is primarily because of their wide bandgap, large conduction band offset, and high carrier mobility. It thus helps in creation of larger PVRs and quantum behaviour at much higher temperature than any other III-V systems. Thus such devices can offer higher power, higher frequency room-temperature operations than other members of the III-V family.

3.1. Matlab Simulation

An attempt was made to study the current – voltage relation of an AlGaN / GaN / AlGaN resonant tunnelling diode using the transfer matrix method described in Chapter 2. The barriers and wells in all applied field calculations were divided into 30 divisions, which should be enough when the barriers and wells are simply trapezoid.

For calculations, a double barrier field structure comprised of $Al_{0.2}Ga_{0.8}N$/ GaN / $Al_{0.2}Ga_{0.8}N$ was considered. The width of each barrier was considered to be 1.50nm and each well was assumed to be of 1.25nm in width. The tunnelling diode was assumed to be grown on a GaN substrate which had a uniform n-type doping of 3.0e19/m^3.

Upon calculations, we obtained a Fermi Energy of $E_f = 0.29$ eV with respect to the conduction band energy of GaN. The electron effective mass of used for GaN was 0.20 me [13]. The Energy band gap of GaN was assumed to 3.42 eV and that of $Al_{0.2}Ga_{0.8}N$ was hence calculated to be 3.866 eV [14]. This, along with conduction band offset of 70% gave the barrier height equal to 0.312 eV.

To obtain the graphs the transmission coefficients were calculated for energies between 0.0006 eV and E_f using 1000 points in the interval. This was done for all potentials varying from 0 to 1.5 V using 250 points in this interval. The calculated current is in arbitrary units, therefore the graph doesn't give any information about the actual current, but only the current-voltage relation for the diode. In the calculation, it has been assumed that the potential drop across the well and the barrier is linear. The graph is plotted on logarithmic scale.

To calculate the value of current, summation was carried on instead of performing integration.

Figure 3.1 shows the current as a function of applied voltage. The important feature to note in this figure is that the current is peaked at a certain voltage. This is where resonance occurs. The region that follows is where the negative differential resistance (NDR) occurs, the current drops when the applied voltage increases. The negative difference region is where the Fermi level has crossed the energy of one of the quasi-bound states in the well.

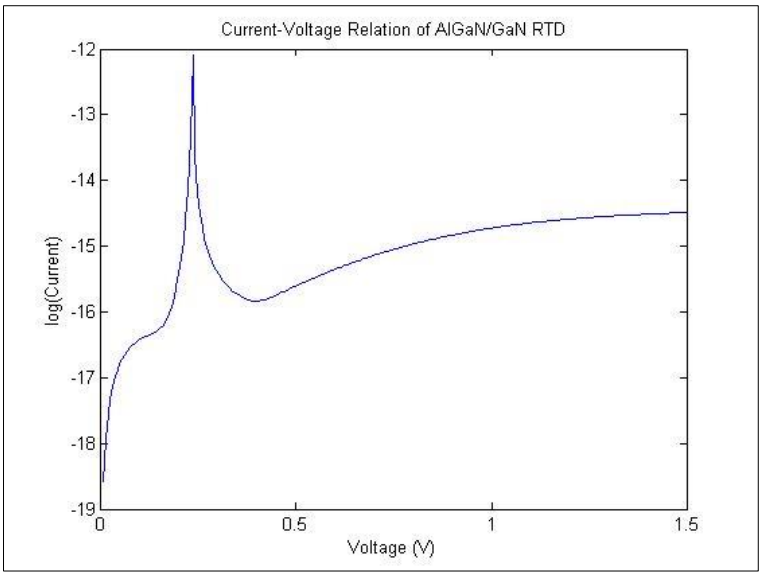

Figure 3.1 Current- Voltage Relation of AlGaN / GaN

3.2. Simulation on ATLAS

After having performed simulation of $Al_{0.2}Ga_{0.8}N$/ GaN / $Al_{0.2}Ga_{0.8}N$ on Matlab and understanding the nature of the current- voltage relation, simulation was performed on ATLAS platform, which is a device simulator, for obtaining more realistic current values.

An $Al_{0.2}Ga_{0.8}N$/ GaN / $Al_{0.2}Ga_{0.8}N$ resonant tunnelling diode structure was created with barrier width of 1.50 nm, and well width of 1.25 nm. This was grown on a GaN substrate of 502nm width. Another GaN layer of width 302 nm was grown on the tunnelling diode. A layer of GaN of width 2nm was kept as spacer on either side of the tunnelling diode. The rest of the GaN substrate was doped with n-type atoms with concentration 3.0e19/m^3. The alignment for conduction band offset was kept at 0.7 (default ATLAS value). Figures 3.2 – 3.5 show the structural properties of the RTD created.

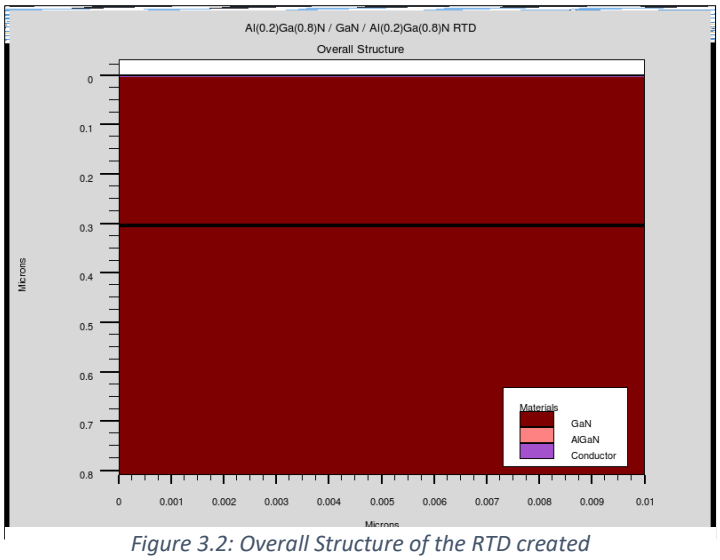

Figure 3.2: Overall Structure of the RTD created

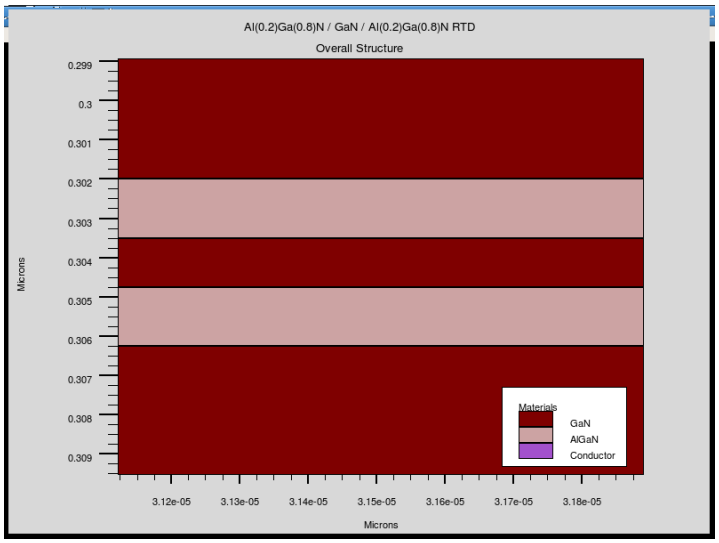

Figure 3.3 : A Zoomed-in view near the RTD region

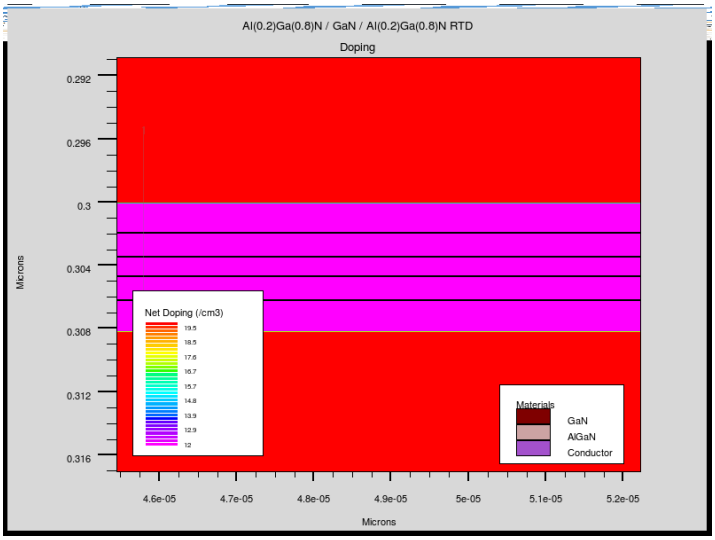

Figure 3.4: Doping Concentration

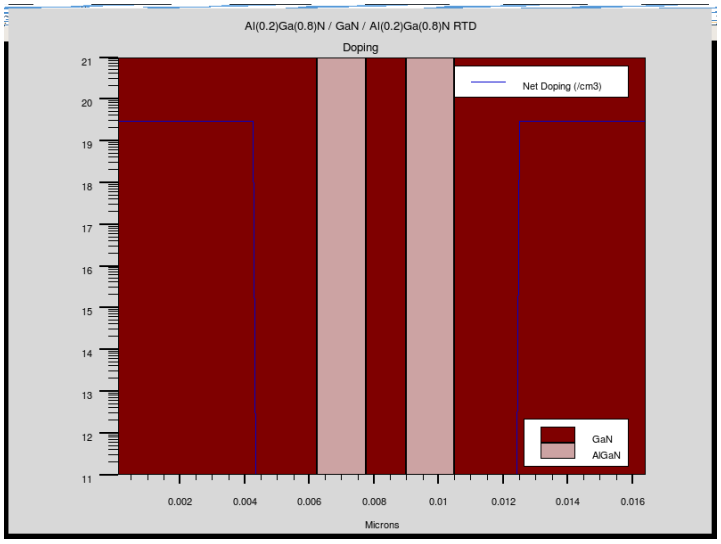

Figure 3.5: Doping Concentration across cut-line

The III-V nitride heterostructures, by virtue of their wurtzite crystal structure and high degree of iconicity, exhibit a variety of material properties that either are not found or are of considerably reduced importance in conventional zinc blende III-V semiconductors. The large iconicity and the large piezoelectric coefficient in group III nitride results in intensive piezoelectric and spontaneous effects in nitride heterostructures due to non-centosymmetry. Piezoelectric effects have been shown to influence carrier distributions, electric fields and consequently a wide range of optical and electronic properties of nitride materials and devices. The ability to achieve two-dimensional electron gases (2DEG) with sheet carrier concentrations of 10^{13} cm^{-2} or higher, close to the interface without any intentional doping contributes to the outstanding performance of AlGaN/GaN based RTDs in a major way.

Hence, a polarization induced sheet charge density = 1.10809e13 cm^{-2} was calculated [15–16] and added to the AlGaN/GaN interfaces to take into account effects due to both polarization and spontaneous charges. The value of polar.scale was set to 0.1 to necessitate proper band bending due to polarization charges. The potential across the collector and the emitter was then varied from 0 to 1.4 V and its effect on the collector current was observed. Figure 3.6 gives the corresponding current-value graph.

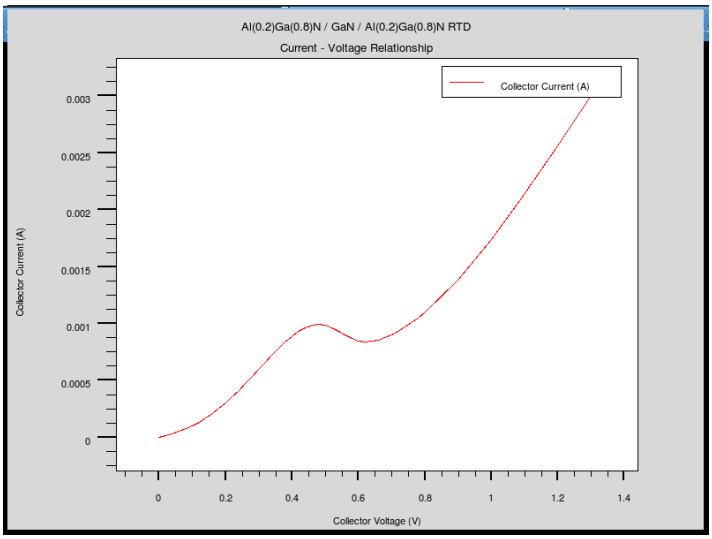

Figure 3.6: I-V curve of AlGaN / GaN / AlGaN

From the graph, we notice that current reaches a maximum value of 1mA at around 0.5V. It then keeps on decreasing till it reaches a minimum value of around 0.83 mA at around 0.6V. Thus we see that a prominent Negative Differential Region is formed. Beyond the valley, the current keeps on increasing because one of the barriers now lie completely below the Fermi Level. Hence, the incident electron reflects only from one barrier and current keeps on increasing. However after a certain voltage, energy of the incident electron becomes more than the barrier height. Beyond this, current keeps on increasing primarily because of thermionic emission.

The devised RTD also gives us a PVR of 1.2.

Figures 3.7 – 3.10 depicts the band diagrams when different potentials are applied across the RTD. The bending of the band is caused by the introduction of polarization charges across the AlGaN/GaN interfaces.

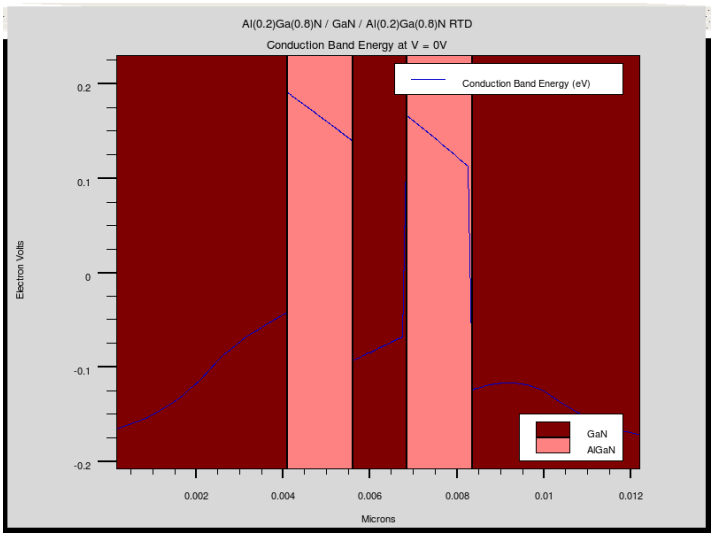

Figure 3.7: Conduction Band Energy when V = 0V

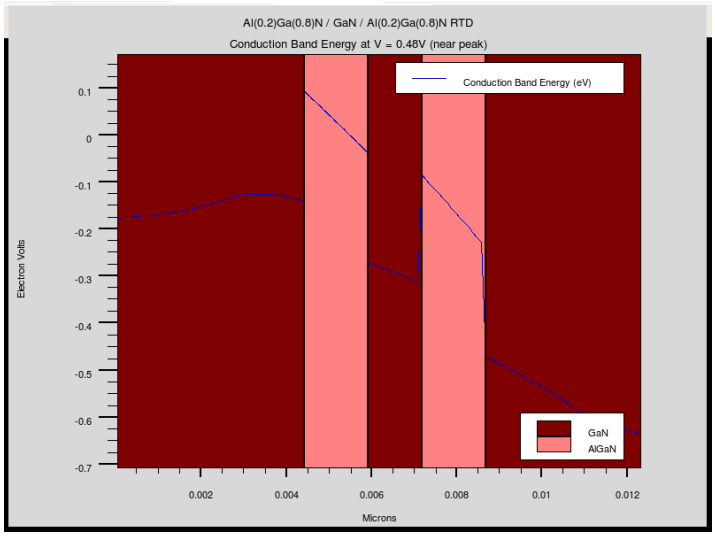

Figure 3.8: Conduction Band Energy when V = 0.48V (near peak)

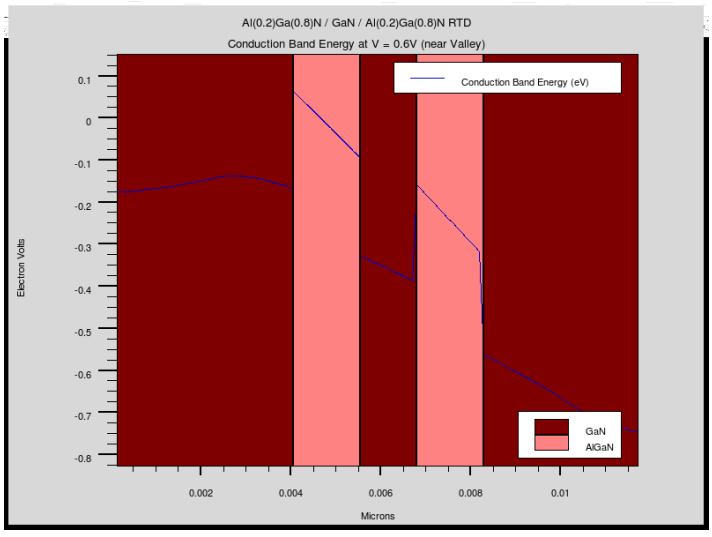

Figure 3.9: Conduction Band Energy when V = 0.6V (near valley)

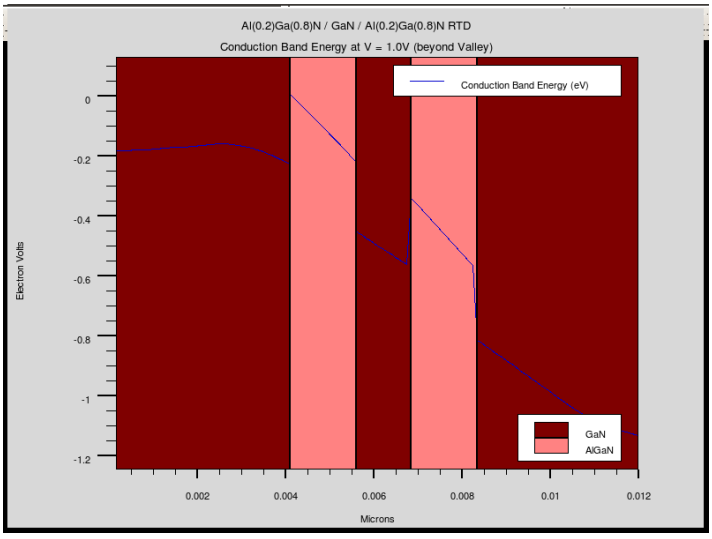

Figure 3.10: Conduction Band Energy when V = 1.0V (beyond valley)

3.3. Current Variation with Al concentration

Following the study of Collector current characteristics of an $Al_{0.2}Ga_{0.8}N$/ GaN / $Al_{0.2}Ga_{0.8}N$ resonant tunnelling diode, the Current-Voltage characteristics of AlGaN /GaN RTDs with different concentrations of Al were compared. Figure 3.11 gives the corresponding result. As expected, with increase in Al concentration, corresponding bandgap of AlGaN increased, which means greater barrier height. As a result, current values decreased considerably and peaks were obtained at higher potentials because incident electrons now needed more energy to reach the quasi-bound energy levels. We also observed an increase in PVR with increase in Al conc. Polarization charge also increased due to increase in piezoelectric charges resulting from an increased lattice mismatch.

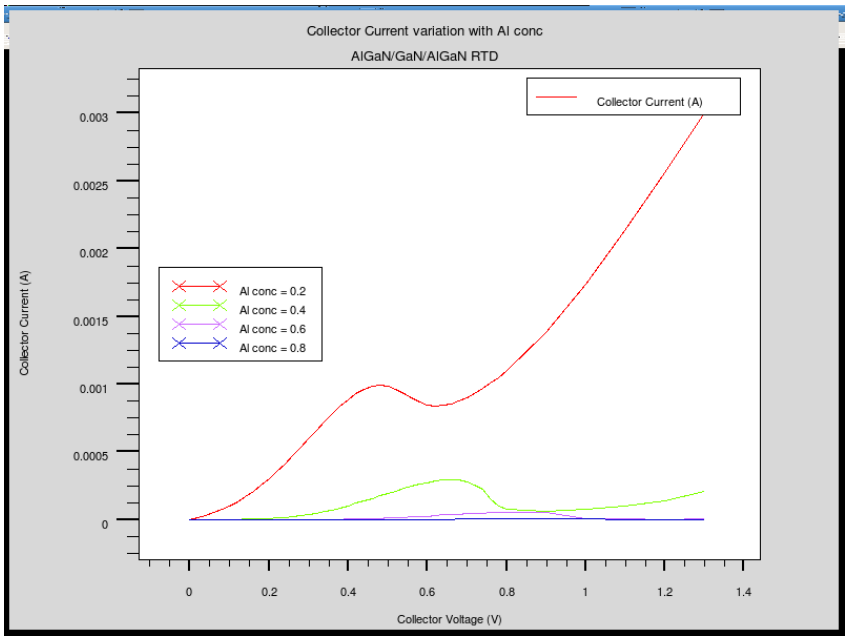

Figure 3.11: Collector Current Variation with Al Conc

3.4. Current Variation with Barrier Width

Figure 3.12 shows the effect of barrier width on the collector-current of $Al_{0.2}Ga_{0.8}N$/ GaN / $Al_{0.2}Ga_{0.8}N$ resonant tunnelling diode. We notice that with increase in barrier width, current decreases. This is primarily because with increase in barrier width, incident electrons encounter increased resistance. Hence they are more likely to be reflected back or absorbed than transmitted. PVR remains almost constant. Energy of quasi-bound levels remain more or less constant, hence, we do not notice much deviation of the voltage at which resonance is achieved.

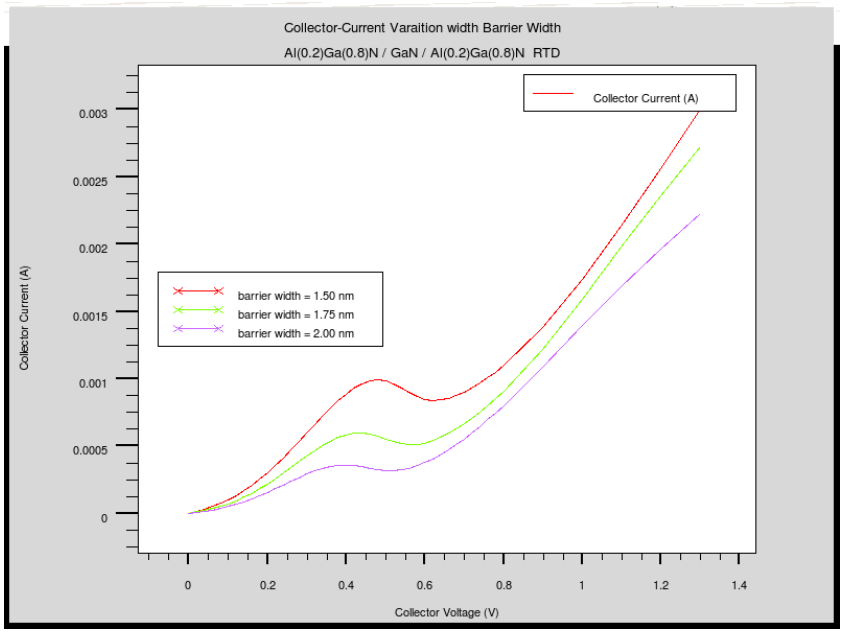

Figure 3.12: Collector Current Variation with Barrier Width

3.5. Current Variation with Well Width

Variation of Collector Current in an $Al_{0.2}Ga_{0.8}N$/ GaN / $Al_{0.2}Ga_{0.8}N$ resonant tunnelling diode with well width was also studied. The corresponding graph is shown in Figure 3.13. We observe that with increase in well width, collector current decreases. This is because with increase in well width, the energy of the electron wave decreases due to increase in propagation distance. A decrease in potential at which resonance occurs is also observed, primarily because increase in well width results in decrease in the quasi-bound energy levels. PVR remains more or less constant.

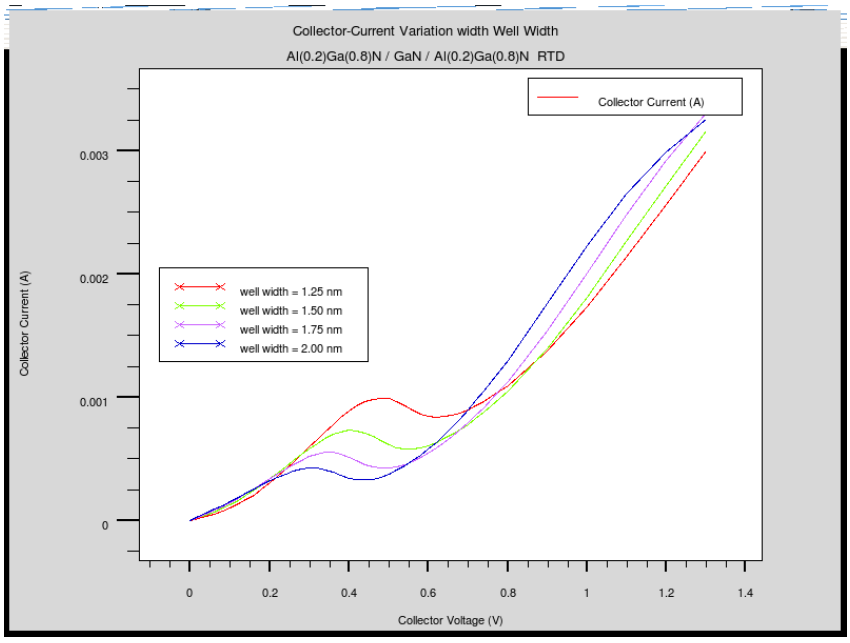

Figure 3.13: Collector Current Variation with Well Width

Chapter 4 : AlInN / GaN / AlInN Resonant Tunneling Diode

As discussed in Chapter 3, the lattice mismatch and strain between AlGaN and GaN layers in AlGaN / GaN RTDs gives rise to the much undesired piezoelectric polarization charges across the interfaces which eventually degrades the performance of RTD by providing asymmetric current voltage characteristics. Therefore, in order to get a reliable, reproducible Negative differential region as well as symmetric current-voltage characteristics, it is absolutely necessary to use a material which would minimise lattice mismatch and hence reduce strain, thereby reducing piezoelectric polarization charges. $Al_{0.83}In_{0.17}N$ alloy which have lattice constant = 3.187 Å [19], is thereby lattice-matched with GaN (lattice constant = 3.190 Å [19]), and thus has spontaneous polarization larger than total of spontaneous and piezoelectric polarization in typical AlGaN / GaN heterostructure. This large polarization discontinuity between AlInN and GaN, which results in a higher 2DEG charge density at the interface, and the lack of strain in AlInN reduces device degradation processes and lead to better structure and reliability.

4.1. Matlab Simulation

The current – voltage relation of an AlInN / GaN / AlInN resonant tunnelling diode using the transfer matrix method described in Chapter 2. The barriers and wells in all applied field calculations were divided into 30 divisions, which should be enough when the barriers and wells are simply trapezoid.

For calculations, a double barrier field structure comprised of $Al_{0.83}In_{0.17}N$ / GaN / $Al_{0.83}In_{0.17}N$ was considered. The width of each barrier was considered to be 1.50nm and each well was assumed to be of 1.25nm in width. The tunnelling diode was assumed to be grown on a GaN substrate which had a uniform n-type doping of 3.0e19/m^3.

Upon calculations, we obtained a Fermi Energy of $E_f = 0.29\ eV$ with respect to the conduction band energy of GaN. The electron effective mass of used for GaN was 0.20 me [13]. The Energy band gap of GaN was assumed to 3.42 eV and that of $Al_{0.83}In_{0.17}N$ was calculated to be 4.02 eV [10]. This, along with valence band offset of 0.2 eV gave the barrier height equal to 0.40 eV.

To obtain the graphs the transmission coefficients were calculated for energies between 0.0006 eV and E_f using 1000 points in the interval. This was done for all potentials varying from 0 to 1.5 V using 250 points in this interval. The calculated current is in arbitrary units, therefore the graph doesn't give any information about the actual current, but only the current-voltage relation for the diode. In the calculation, it has been assumed that the potential drop across the well and the barrier is linear. The graph is plotted on logarithmic scale.

To calculate the value of current, summation was carried on instead of performing integration.

Figure 4.1 shows the current as a function of applied voltage. The important feature to note in this figure is that the current is peaked at a certain voltage. This is where resonance occurs. The region that follows is where the negative differential resistance (NDR) occurs, the current drops when the applied voltage increases. The negative difference region is where the Fermi level has crossed the energy of one of the quasi-bound states in the well.

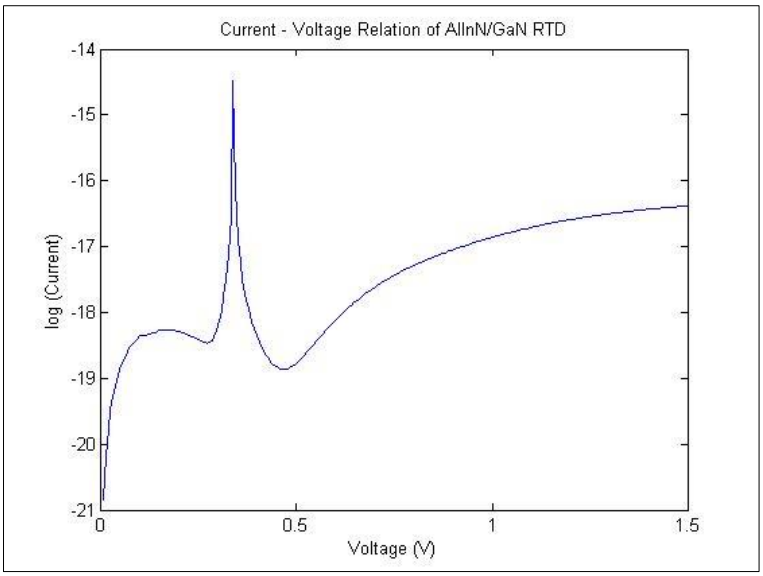

Figure 4.1: Current – Voltage Relation of AlInN/GaN RTD

4.2. Simulation on ATLAS

After having performed simulation of $Al_{0.83}In_{0.17}N$ / GaN / $Al_{0.83}In_{0.17}N$ on Matlab and understanding the nature of the current- voltage relation, simulation was performed on a device simulator platform ATLAS, for obtaining more realistic current values.

An $Al_{0.83}In_{0.17}N$ / GaN / $Al_{0.83}In_{0.17}N$ resonant tunnelling diode structure was created with barrier width of 1.50 nm, and well width of 1.25 nm. This was grown on a GaN substrate of 502nm width. Another GaN layer of width 302 nm was grown on the tunnelling diode. A layer of GaN of width 2nm was kept as spacer on either side of the tunnelling diode. The rest of the GaN substrate was doped with n-type atoms with concentration 3.0e19/m^3. The alignment for conduction band offset was kept at 0.67 (as reported in section 4.1). Figures 4.2 – 4.5 show the structural properties of the RTD created.

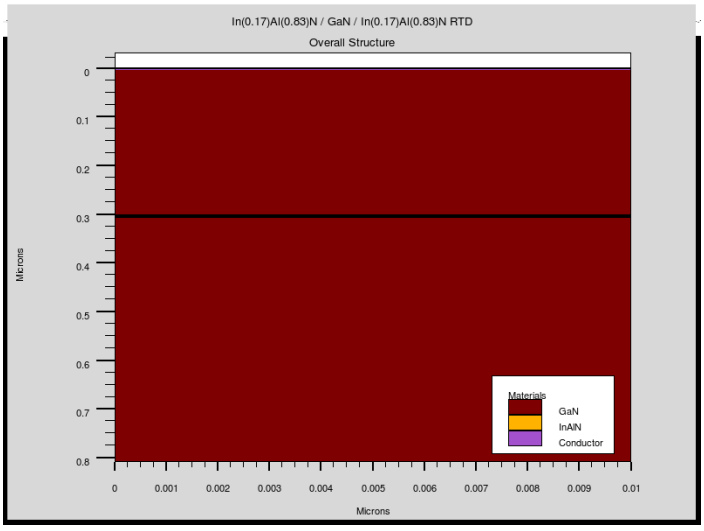

Figure 4.2: Overall Structure of AlInN/GaN RTD

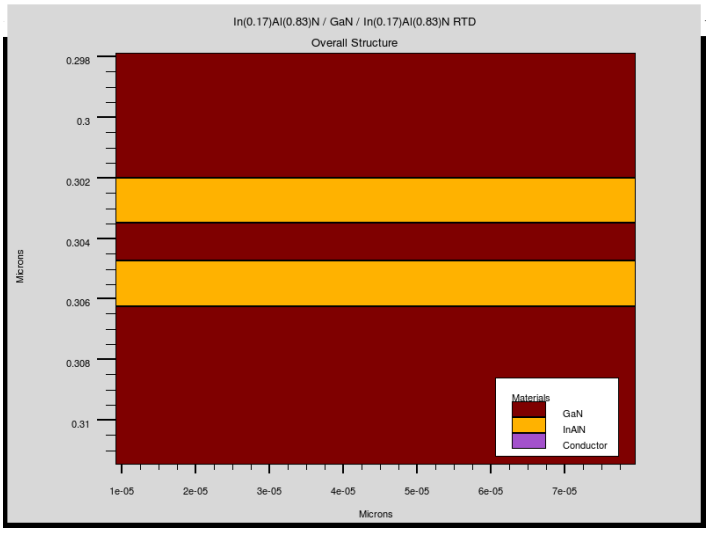

Figure 4.3: A Zoomed-in view near the RTD region

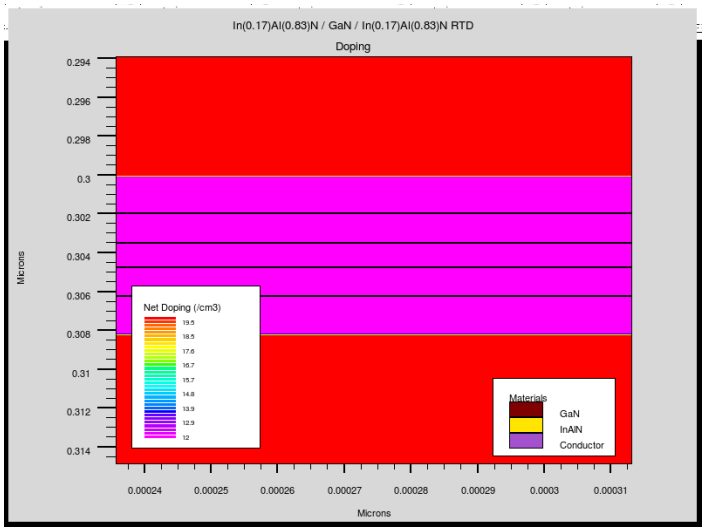

Figure 4.4: Doping Concentration

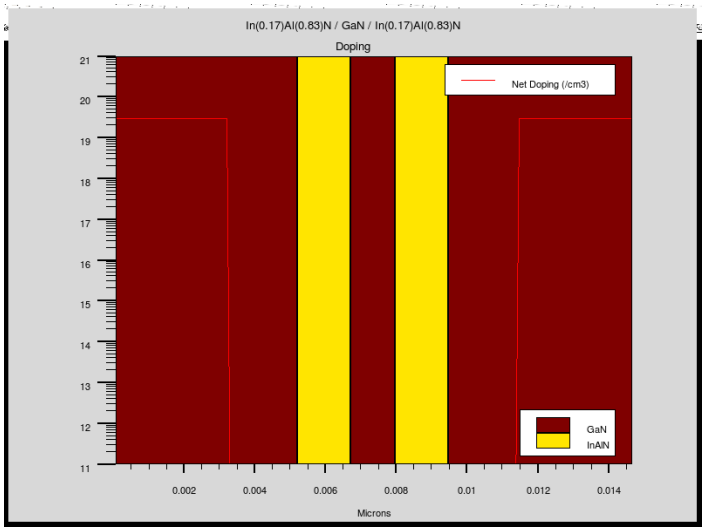

Figure 4.5: Doping Concentration across Cut-line

As already discussed previously, AlInN being a member of III-V heterostructure family, it shows prominent polarization effects. However, $Al_{0.83}In_{0.17}N$ being lattice-matched to GaN, piezoelectric polarization charges which results from strain in lattice, becomes negligible. However the spontaneous polarization charge becomes very significant.

Hence, A polarization induced sheet charge density = 2.69e13 cm^{-2} was calculated [19] and added to the AlInN/GaN interfaces to take into account effects due to both polarization and spontaneous charges. The value of polar.scale was set to 0.1 to necessitate proper band bending due to polarization charges. The potential across the collector and the emitter was then varied from 0 to 1.4 V and its effect on the collector current was observed. Figure 4.6 gives the corresponding current- value graph.

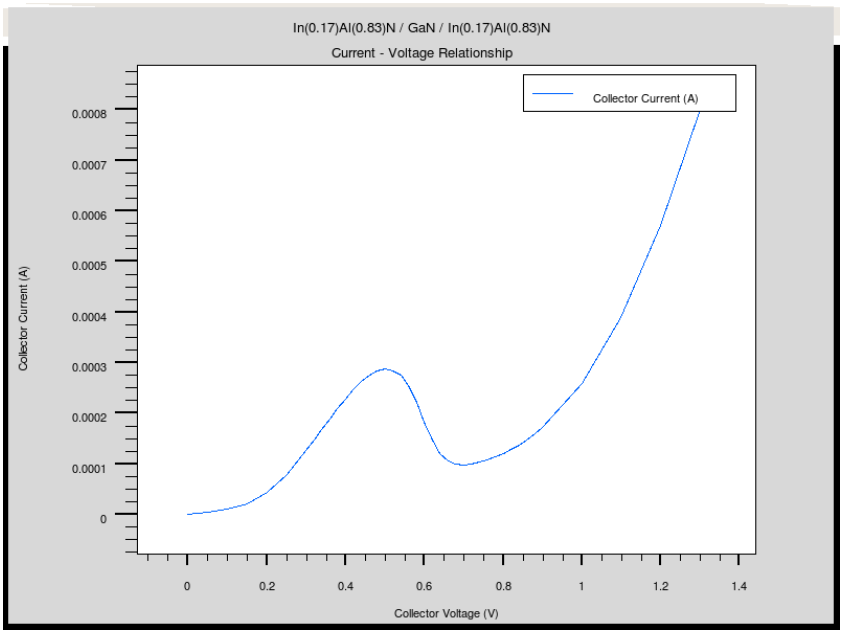

Figure 4.6: I-V curve of AlInN / GaN / AlInN

From the graph, we notice that current reaches a maximum value of 0.3mA at around 0.5V. It then keeps on decreasing till it reaches a minimum value of around 0.1 mA at around 0.7V. Thus we see that a prominent Negative Differential Region is formed. Beyond the valley, one of the barriers now lie completely below the Fermi Level. Hence, the incident electron reflects only from one barrier and current keeps on increasing. However after a certain voltage, energy of the incident electron becomes more than the barrier height. Beyond this, current keeps on increasing primarily because of thermionic emission.

The devised RTD also gives us a PVR of 3.

Figures 4.7 – 4.10 depicts the band diagrams when different potentials are applied across the RTD. The bending of the band is caused by the introduction of polarization charges across the AlInN/GaN interfaces.

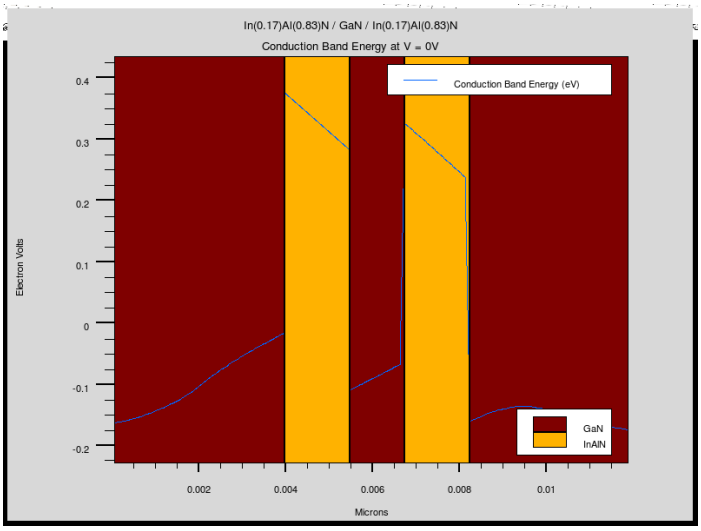

Figure 4.7: Conduction Band Energy when V = 0V

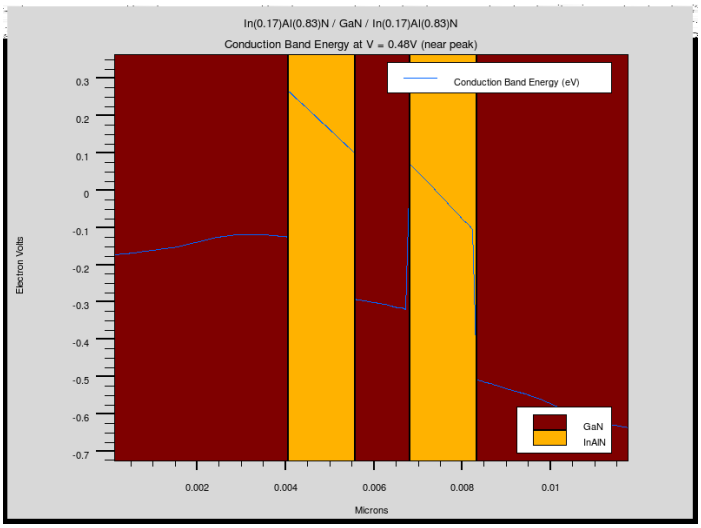

Figure 4.8: Conduction Band Energy when V = 0.48V (near peak)

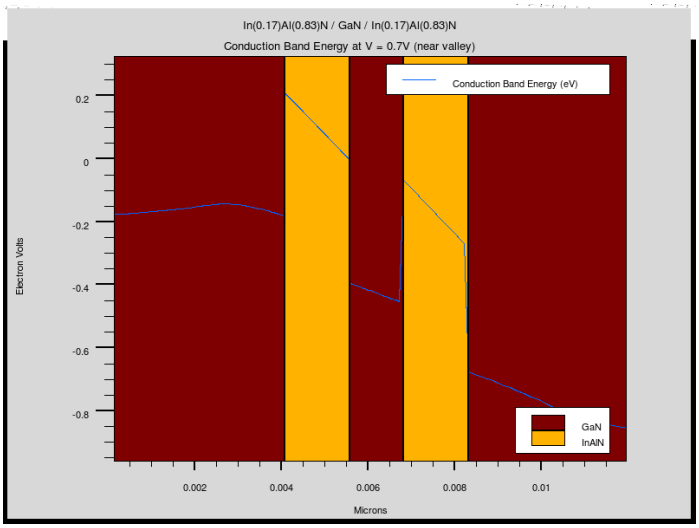

Figure 4.9: Conduction Band Energy when V = 0.7V (near valley)

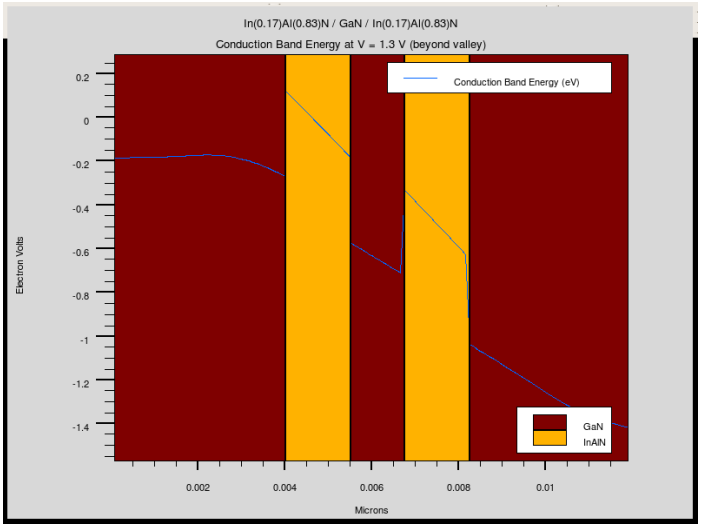

Figure 4.10: Conduction Band Energy when V = 1.3V (beyond valley)

4.3. Current Variation with Barrier Width

Figure 4.11 shows the effect of barrier width on the collector-current of $Al_{0.83}In_{0.17}N$/ GaN / $Al_{0.83}In_{0.17}N$ resonant tunnelling diode. We notice that with increase in barrier width, current decreases. This is primarily because with increase in barrier width, incident electrons encounter increased resistance. Hence they are more likely to be reflected back or absorbed than transmitted. PVR remains almost constant. Energy of quasi-bound levels remain more or less constant, hence, we do not notice much deviation of the voltage at which resonance is achieved.

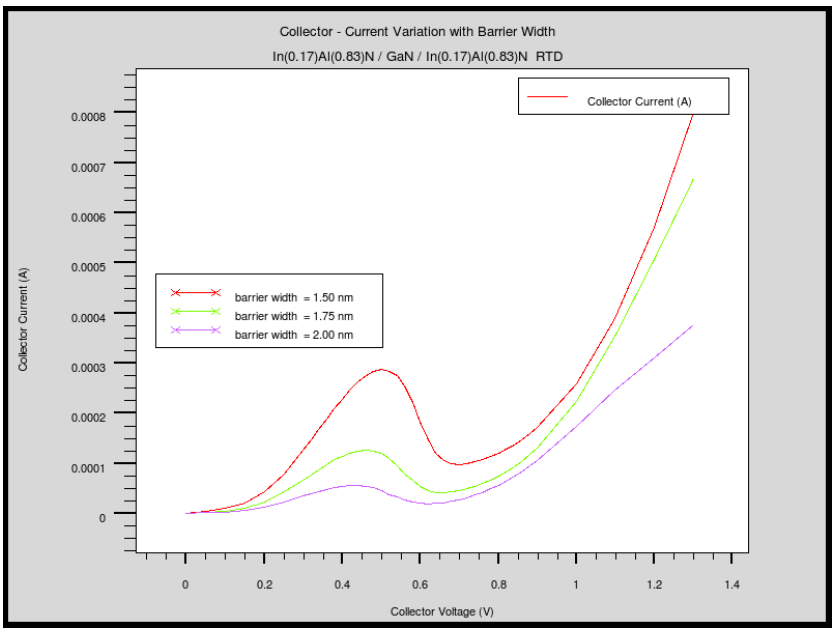

Figure 4.11: Collector Current Variation with barrier width

4.4. Current Variation with Well Width

Variation of Collector Current in an $Al_{0.83}In_{0.17}N$/ GaN / $Al_{0.83}In_{0.17}N$ resonant tunnelling diode with well width was also studied. The corresponding graph is shown in Figure 4.12. We observe that with increase in well width, collector current decreases. This is because with increase in well width, the energy of the electron wave decreases due to increase in propagation distance. A decrease in potential at which resonance occurs is also observed, primarily because increase in well width results in decrease in the quasi-bound energy levels. However, the PVR remains more or less constant.

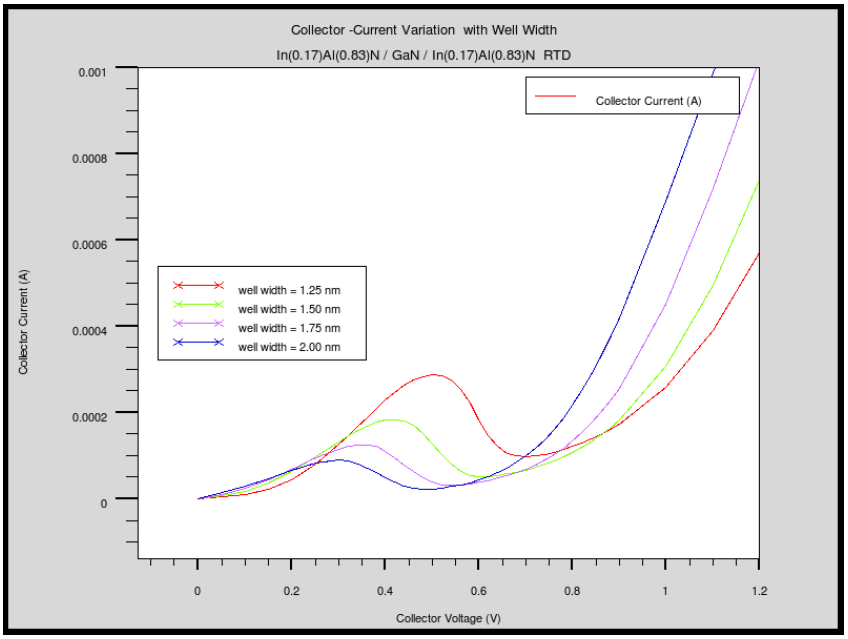

Figure 4.12: Collector Current Variation with Well Width.

Conclusion

We observe that in case of AlGaN/ GaN RTDs, current – voltage characteristics deteriorates and loses its symmetry as concentration of Al in the ternary compound rises. The negative differential region is also observed to become less reliable and less stable. This is primarily because, with increase in Al concentration, lattice constants of the ternary compounds increases. This leads to an increased lattice mismatch with the GaN substrate. As a result, strain is developed at the AlGaN / GaN interface resulting in increased amounts of piezoelectric polarization charges, which thus degrades the performance of RTDs by asymmetric current- voltage characteristics. Therefore, reducing the Al conc (0.2) during growth process is expected to give better current- voltage characteristics.

The $Al_{0.83}In_{0.17}N$ ternary alloy on the other hand has lattice constants almost equal to those of the GaN substrate. Due to lattice matching, strain is greatly reduced across the interface, hence piezoelectric polarization charge becomes negligible. However, its spontaneous charge becomes more that the total polarization charge in $Al_{0.2}Ga_{0.8}N$ / GaN RTD. This means a higher 2DEG density at interfaces. As a result of both these effects, device degradation is significantly reduced, current-voltage characteristics become more symmetric and NDR becomes more stable and reliable.

If we compare both AlInN and AlGaN current characteristics (Figure 4.6 and Figure 3.6 respectively), we notice that current in AlInN has a prominent NDR region with a high PVR of 3 compared to AlGaN which has a PVR of 1.2. Peak Current is observed at 0.48V for both AlInN and AlGaN, whereas Valley Current is observed at 0.6V for AlGaN and 0.7V for AlInN. These imply that NDR in AlInN is more stable than in AlGaN. A lower current value is also observed for AlInN, which is attributed to the higher conduction band offset and increase in 2DEG charge densities at interfaces. However it is not of much significance since AlInN leads to a more symmetric current-voltage characteristic compared to AlGaN as is visible from the graphs.

References

[1] Ben G. Streetman, Sanjay Kumar Banerjee, “Solid State Electronic Devices”, Sixth Edition, PHI Learning Private Limited.

[2] Mustafa K.Ozturk, Engin Arslan, Ilknur Kars, Suleyman Ozcelik, and Ekme lOzbay, “Strain analysis of the GaN epitaxial layers grown on nitridated Si(111) substrate by metal organic chemical vapour deposition”, *Materials Science in Semiconductor Processing,* Volume 16, Issue 1, (Feb 2013): 83‑88.

[3] V. S. Harutyunyan, A. P. Aivazyan, E. R. Weber, Y. Kim, Y. Park and S. G. Subramanya, “High-resolution x-ray diffraction strain-stress analysis of GaN/sapphire heterostructures”, *Journal of Physics D: Applied Physics*, Volume 34, Issue 10A, (2001) A35 - A39.

[4] M. O. Vassell, Johnson Lee, and H. F. Lockwood, “Multibarrier tunneling in Ga1−xAlxAs/GaAs heterostructures”, *Journal of Applied Physics,* Volume 54, Issue 9, (Sept 1983): 5206 – 5213.

[5] Johnny Ling, “Resonant Tunneling Diodes: Theory of Operation and Applications”, University of Rochester, Rochester, NY 14627

[6] I. Hase, H. Kawai, K. Kaneko, and N. Watanabe, “Current–voltage characteristics through GaAs/AlGaAs/GaAs heterobarriers grown by metalorganic chemical vapor deposition”, *Journal of Applied Physics,* Volume 59, Issue 11, (Jun 1986): 3792 – 3797.

[7] R. Tsu and L. Esaki, “Tunneling in a finite superlattice”, *Applied Physics Letters 22*, (1973): 562 - 564.

[8] David Yuk Kei Ko and J. C. Inkson, “Matrix method for tunneling in heterostructures: Resonant tunneling in multilayer systems”, *Physical Review B 38,* (15 Nov, 1988): 9945 – 9951.

[9] R. R. Pelá, C. Caetano, M. Marques, L. G. Ferreira, J. Furthmüller, and L. K. Teles, “Accurate band gaps of AlGaN, InGaN, and AlInN alloys calculations based on LDA - 1/2 approach”, *Applied Physics Letters,* Volume 98, Issue 15, (Apr 2011) : 151907 – 151907-3.

[10] E. Iliopoulos, A. Adikimenakis, C. Giesen, M. Heuken, and A. Georgakilas, “Energy bandgap bowing of InAlN alloys studied by spectroscopic ellipsometry”, *Applied Physics Letter* 92, (2008): 191907 – 191907-3.

[11] C. Mietze, K. Lischka, and D. J. As, “Current – Voltage characteristics of cubic Al(Ga)N/GaN double barrier structures on 3C- SiC”, *Physica Status Solidi A 209*, No. 3, (2012): 439 – 442.

[12] Haoran Chen, Lin’an Yang, Shuang Long, and Yue Hao, “Reproducibility in the negative differential resistance characteristic of In0.17Al0.83N/GaN resonant tunneling diodes – Theroretical investigation”, *Journal of Applied Physics 113,* (2013): 194509 – 194509-7.

[13] Wen Bo *et al*, “Influence of Polarization Effects on the Energy Band of AlGaN / GaN / AlGaN Heterostructures”, *Chinese Physics Letters 21, (*2004): 720.

[14] N. Grandjean, B. Damilano, S. Dalmasso, M. Leroux, M. Laügt, and J. Massies, “Built-in electric-field effects in wurtzite AlGaN/GaN quantum wells”, *Journal of Applied Physics 86,* (1999): 3714

[15] E. T. Yu, X. J. Dang, P. M. Asbeck, S. S. Lau and G. J. Sullivan, “ Spontaneous and piezoelectric polarization effects in III – V nitride heterostructures”, *J. Vac. Sci. Technol. B 17*, (1999): 1742.

[16] O. Ambacher, J. Smart, J. R. Shealy, N. G. Weimann, K. Chu, M. Murphy, W. J. Schaff, L. F. Eastman, R. Dimitrov, L. Wittmer, M. Stutzmann, W. Rieger, and J. Hilsenbeck, “Two-dimensional electron gases induced by spontaneous and piezoelectric polarization charges in N- and Ga-face AlGaN/GaN heterostructures”, *Journal of Applied Physics 85*, (1999): 3222

[17] M. Neuburger, T. Zimmermann, E. Kohn, A. Dadgar, F. Schulze, A. Krtschil, M. Gunther, H. Witte, J. Blasing, A. Krost, I. Daumiller, M. Kunze, R. E. Leoni, “Unstrained InAlN/ GaN HEMT structure”, *High Performance Devices, Proceedings,* 161-166.

[18] M. Akazawa, B. Gao, T. Hashizume, M. Hiroki, S. Yamahata, and N. Shigekawa, “Measurement of valence-band offsets of InAlN/GaN heterostructures grown by metal-organic vapour phase epitaxy”, *Journal of Applied Physics 109,* (2011): 013703.

[19] O. Ambacher *et al*, “Pyroelectric properties of Al(In)GaN/GaN hetero- and quantum well structures”, *Journal of Physics: Condensed Matter 14*, (2002): 3399 – 3434.